The effect of hydrophobic and hydrophilic channel walls on the structure and diffusion of water and ions

T. W. Allen[a)]
Protein Dynamics Unit, Department of Chemistry, Australian National University, Canberra, ACT 0200, Australia

S. Kuyucak
Department of Theoretical Physics, Research School of Physical Sciences, Australian National University, Canberra, ACT 0200, Australia

S.-H. Chung
Protein Dynamics Unit, Department of Chemistry, Australian National University, Canberra, ACT 0200, Australia

(Received 8 June 1999; accepted 10 August 1999)

Molecular dynamics simulations are carried out to determine the effects of channel wall structure on water and ion properties. We compare hydrophobic (Lennard-Jones 5-3 and atomic) and molecular-hydrophilic cylindrical pores of 2–6 Å in effective radius, relevant to the study of most significant biological ion channels including gramicidin A, ACh, and potassium channels, and to the study of many microporous materials. Large variations in levels of self-diffusion and rotational correlation within hydrophobic channels are explained in terms of water geometry, hydrogen bonding, and dipole correlation. The differing levels of water structure and self-diffusion in hydrophobic and hydrophilic pores arise because of marked differences in the preferred orientation of water dipole moments, and due to hydrogen bonding with molecules on the pore lining. Axial sodium ion diffusion does not experience large variations with pore size, despite anomalous stability in moderate-sized hydrophobic pores. We attribute this to the ability of ions to diffuse along troughs of water density. Ion diffusion along the pore axis exhibits a general increase with channel radius in hydrophobic channels but remains fairly low in hydrophilic channels. © *1999 American Institute of Physics.* [S0021-9606(99)51541-9]

I. INTRODUCTION

Diffusion of water and ions in molecular-sized pores is an important problem in many areas of research ranging from biology (e.g., ion channels in membranes[1]) to chemistry and chemical engineering (e.g., zeolites and silicates[2,3]). There are large variations in the size and constitution of pores, and one intuitively expects these variations to have a significant impact on the water and ion structure and transport properties. For example, biological ion channels may be lined with mostly hydrophobic amino acids, such as in the ACh channel,[4] mostly hydrophilic residues such as in gramicidin A,[5] or a combination, as recently discovered for the potassium channel.[6] These channels also vary in dimension from the narrow gramicidin, with radius approximately 2 Å, to the wider nicotinic ACh receptor having radius of the order 3–6 Å, and bacterial porin larger than 10 Å in radius (see, e.g., Tieleman and Berendsen[7]). Therefore, it is important that the effects of both the pore size and the pore constitution on water and ion structure and dynamics within these channels is understood.

When simulating ions in channels with continuum methods, such as Poisson–Boltzmann and Poisson–Nernst–Planck, and stochastic dynamics, such as Brownian dynamics, channel water is not implemented. Instead, one introduces a mean ion mobility reflecting the ability of an ion to diffuse under the action of systematic and random forces. Until recently there has been little knowledge about the variation in ion diffusion coefficient with channel constitution and size, and very little understanding of the mechanisms underlying these dependencies. Studies exist which examine the effect of a confining, exponentially repulsive wall on water structure and diffusion[8] and ion diffusion[9] within cylindrical channels. However, there remains little investigation into the effects of realistic channel pores on ion diffusion, except for the occasional ion diffusion estimate for particular channel systems such as model ACh channels,[10] and gramicidin.[11] Here we report the results of systematic molecular dynamics (MD) simulations within atomic-hydrophobic and molecular-hydrophilic channels, providing microscopic explanations for the channel water structure, self-diffusion, and sodium ion diffusion. The latter will be especially useful in constraining the range of ion diffusion parameters used in the more phenomenological approaches mentioned above.

In large biological ion channels, hydrophobic segments can account for a majority of the protein residues lining the pore. Representing these hydrophobic segments with one-dimensional potential functions can appreciably speed up MD simulations. Until now only Lennard-Jones (LJ) potential functions for planar hydrophobic surfaces have been

a)Electronic mail: Toby.Allen@anu.edu.au

available for this purpose (see, e.g., Lee, McCammon, and Rossky[12]). We introduce a new LJ potential function optimized for use in pore situations with radii ranging from 2.1 to 6.1 Å. This LJ potential will be useful in speeding up computer simulation studies of biological ion channels and microporous materials.

The paper is arranged as follows: We first introduce our model channels, simulation protocols, and analysis procedures, and then report and discuss the results of these MD simulations. To understand variations in water self-diffusion with channel wall type and size, we investigate the packing of water molecules in these channels. The packing is revealed in terms of the ordering of water molecules into disks, shells, and columns. In particular, the dipole correlations within and between these well-defined regions, and the hydrogen bonding networks are used to explain the translational and rotational freedom of the solvent. We finally discuss ion–water geometry and ion diffusion estimates within the different pore types and report our major findings in Sec. VII.

II. METHODS

A. Model systems

In this study we consider three channel types. The first has a hydrophobic wall consisting of a regular array of LJ 12-6 centers on a cylindrical shell, the second is a structureless one-dimensional potential function which approximates this atomic wall, and the third type is a hydrophilic wall containing an array of bound polar molecules. The hydrophilic wall consists of water molecules at bulk water density with oxygen atoms fixed on a cylindrical grid. The atomic hydrophobic wall is generated with just the oxygen atom LJ 12-6 centers. The atomic grid is designed such that the nearest-neighbor distance s (typically 3.14 Å) on a particular disk, of radius a, is equal to the nearest-neighbor distance between disks on this cylindrical shell, as shown in Fig. 1(A). Because each disk has been rotated with respect to its neighbors so as to maximize the closeness of packing, the disk separation is $d=(\sqrt{3}/2)s$. The volume of this cylindrical shell, extending from radius $a-s/2$ to $a+s/2$, is $4\sqrt{3}\pi^3a^3/N^2$, where N is the number of atoms (or molecules) on each circular disk. Assuming a density of $\rho=1$ g/cm^3, N is given by the nearest integer to $1.93a$. We consider radii a from 3.5 to 7.0 Å in 0.5 Å increments corresponding to effective channel radii 2.1–5.6 Å. This number of oxygen atoms is evenly spaced around the circular disk with separation $s=2\pi a/N$, with each adjacent disk offset by $s/2$. For the chosen values of a, $N=2a$ and therefore $d=(\sqrt{3}/2)a=2.72$ Å for all channel sizes. Water hydrogen atoms are free to rotate around these oxygen atoms in the hydrophilic wall. The effective radius of these cylinders is $R=a-1.4$ Å where the approximate radius of an oxygen atom has been subtracted from the radial position of the atomic centers.

To obtain a one-dimensional hydrophobic potential that depends only on the perpendicular distance from the channel wall, we Boltzmann average the LJ 12-6 potentials due to the array of oxygen atoms. This procedure was previously used for averaging LJ 12-6 potentials due to an array of atoms on a planar surface,[13] which can be approximated with an effective LJ 9-6 potential. For a cylinder with radius R, the Boltzmann averaged potential $V_R^B(r)$ is given by

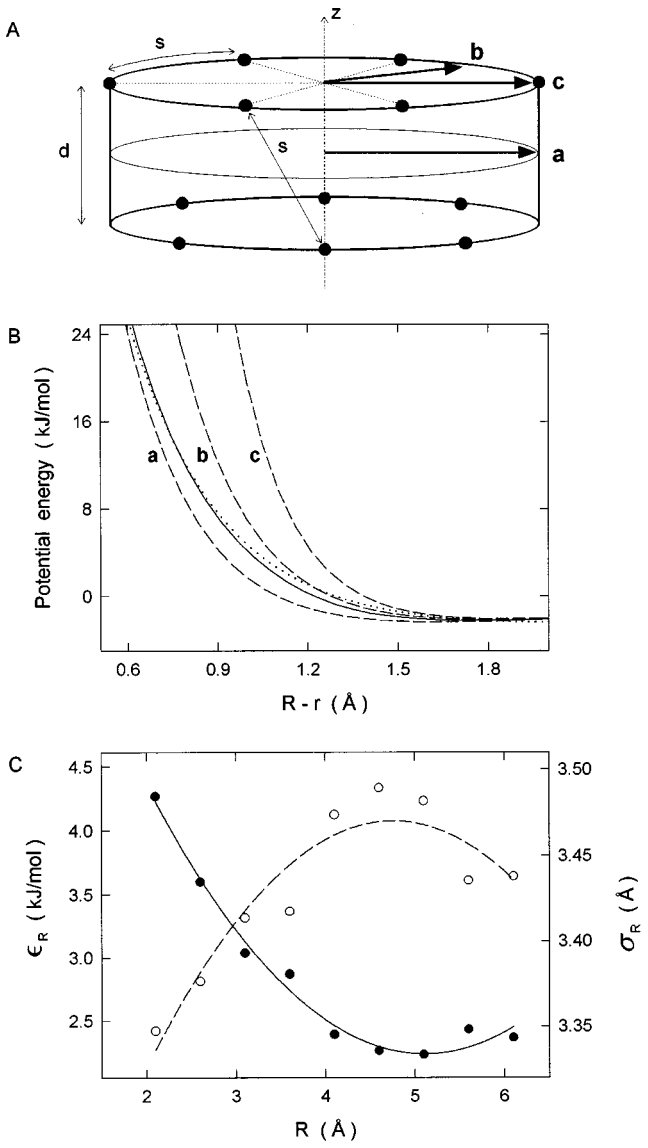

FIG. 1. (A) Atomic wall lattice structure: Two layers of an oxygen atom lattice are drawn for a cylinder containing 6 atoms per layer. The interatomic distance within a layer and between layers (s), and the layer separation (d) are drawn as double headed arrows. The vectors **a**, **b**, and **c** radiating from the channel axis (z) indicate the directions used for demonstration of potential profiles. The vectors are: between layers, directed toward the point directly under one atom (**a**); within a layer, directed at a point midway between neighboring atoms (**b**); and within a layer, directed straight at an atom (**c**). (B) Potential profiles for the $R=4.1$ Å ($a=5.5$ Å) channel. Each layer/disk contains 11 atoms arranged 32.7° apart, separated from adjacent disks by 2.72 Å. The vectors **a**, **b**, and **c** radiate from the channel axis at (ϕ,z) values of (16.36°,0), (16.36°, 1.36 Å), and (0°, 1.36 Å), respectively. Potential profiles for directions **a**, **b**, and **c** (dashed curves) are compared to the Boltzmann averaged potential function (the solid curve). The LJ 5-3 fitting function (3) is shown as a dotted curve. The horizontal axis is the distance from the effective channel radius ($R-r$ where $R=a-1.4$ Å). (C) Lennard-Jones 5-3 parameters: Depth of potential minimum ϵ_R (solid curve, filled circles, left axis) and the position of the potential minimum σ_R (dashed curve, open circles, right axis). Uncertainties in ϵ_R and σ_R are less than 4% and 0.4%, respectively, and thus are not shown.

$$V_R^B(r) = kT \ln\left[\frac{1}{2\pi d}\int_{-d/2}^{d/2} dz \int_0^{2\pi} d\phi e^{-V(r,\phi,z)/kT}\right], \quad (1)$$

where

$$V(r,\phi,z) = \sum_i \epsilon\left[\left(\frac{\sigma}{|\mathbf{r}-\mathbf{r}_i|}\right)^{12} - 2\left(\frac{\sigma}{|\mathbf{r}-\mathbf{r}_i|}\right)^{6}\right]. \quad (2)$$

The sum is carried over all the atoms on the wall at positions $\mathbf{r}_i$, and gives the total potential V at $\mathbf{r}=(r,\phi,z)$. The LJ parameter σ gives the position of the minimum in the LJ 12-6 function, and ϵ is the depth of this minimum. The Boltzmann average involves an integral over the potential due to a total of 19 disks of atoms covering cylindrical segments approximately 51.69 Å in length. The effective one-dimensional potential V_R^B is then fitted by a general LJ function of the form

$$V_R^{\mathrm{LJ}}(\Delta) = \frac{m_R}{n_R - m_R}\epsilon_R\left[\left(\frac{\sigma_R}{\Delta}\right)^{n_R} - \frac{n_R}{m_R}\left(\frac{\sigma_R}{\Delta}\right)^{m_R}\right], \quad (3)$$

where $\Delta = a - r$ is the distance from the channel wall as defined by the atomic centers, and the parameters n_R, m_R, ϵ_R, and σ_R are determined through an iterative least-squares procedure. The function (3) has been designed such that σ_R and ϵ_R correspond to the position and depth of the potential minimum, respectively.

Figure 1(B) compares the Boltzmann averaged potential for a moderate size cylinder of effective radius $R=4.1$ Å with potential curves corresponding to three directional vectors **a**, **b**, and **c** as indicated in Fig. 1(A). Away from the wall, the averaged function provides a good estimate of the potential for all z and ϕ. Closer to the channel wall there exists a noticeable difference between points adjacent to wall atoms and those between atoms. Density profiles, and other structural analysis, to be revealed later in this article, determine by how much these deviations should influence water properties within the channels.

For the range in effective cylinder radii $R=2.1-6.1$ Å, the function (3) is fitted to the Boltzmann averaged potentials. In each case, only a LJ 5-3 potential can be fitted to within the uncertainties in the parameters. The parameters ϵ_R and σ_R obtained from fits of Eq. (3) assuming a LJ 5-3 form are shown in Fig. 1(C). These ϵ_R and σ_R values can be fitted with the quadratic forms in R,

$$\epsilon_R = 7.7760 - 2.2455R + 0.2197R^2 \quad \text{kJ/mol}, \quad (4)$$

and

$$\sigma_R = 3.0414 + 0.180\,34R - 0.018\,95R^2 \quad \text{Å}, \quad (5)$$

as indicated by the solid and dashed curves, respectively, in Fig. 1(C). Note that the variation in σ_R with R is quite small and one can use the average value 3.45 Å. The LJ 5-3 fitting function for the pore size $R=4.1$ Å is shown Fig. 1(B) (dotted line), which gives an adequate representation of the Boltzmann averaged curve (solid line). Similar agreement is seen for the whole range of channel sizes.

B. Simulation details

MD simulations are performed using the CHARMM v25b2 code[14] with modifications. A time step of 1 fs is used with the Verlet MD algorithm.[15] Velocity rescaling at 1 ps intervals leads to temperatures of 300.0 ± 0.5 K, with negligible effect on diffusion. Coordinates are saved each 0.1 ps for trajectory analysis. Periodic boundaries are enforced with a single image placed above and below each channel.

The standard rigid five-site ST2 water model has been employed[16] with LJ 12-6 parameters for the oxygen–oxygen interaction being $\sigma=3.4796$ Å and $\epsilon=0.3170$ kJ/mol. This model is chosen because of its ability to represent water in aqueous solutions accurately across the range of static and dynamic ion and water properties. For example, a bulk water self-diffusion value of 0.285 Å^2/ps has been found for ST2 water,[17] which is in reasonable agreement with the experimental value[18] 0.24 Å^2/ps. Only the SPC/E model provides better agreement with experiment with the value[19] 0.25 Å^2/ps. In the popular TIP3P model,[20] a rather high diffusion constant of 0.40 Å^2/ps arises.[21] This has prompted introduction of a modified TIP3P model with flexible O–H bonds, reducing self-diffusion to a more acceptable level[21] (0.32 Å^2/ps), as employed, for example, in MD simulations of model channels.[8] Such modifications are not needed in ST2. Hydration numbers, radii, and ion–water geometry are well reproduced with the ST2 model for a variety of ion species[17] despite the apparent exaggeration of charge distribution with the five-site model. A drawback of this model is the increased trajectory storage and simulation times associated with the explicit treatment of lone pairs. However, CHARMM offers special fast routines for this water model, overcoming this problem to some degree. Ion–water potential models are available for the ST2 model and LJ 12-6 parameters have been taken from Heinzinger.[17] The Na–water oxygen LJ 12-6 interaction has $\sigma=3.2776$ Å and $\epsilon=0.330$ kJ/mol.

Test simulations reveal that channel length can have a considerable influence on diffusion. Channels of length 50 and 60 Å are found to give indistinguishable levels of self-diffusion in the axial (z) direction, whereas the shorter 40 Å channels have diffusion reduced by approximately 25%. Tests also show that the diffusion does not change noticeably when the periodic ends of this segment are replaced with repulsive constraints. Our structureless hydrophobic wall (LJ 5-3) channels are given a length of 50 Å with periodic boundaries, applied to water molecules and ions, acting at each end. Because of the discrete nature of the wall lattice for the atomic hydrophobic and hydrophilic walls, periodic boundaries are applied at the ends of a 51.69 Å segment.

The treatment of long-range forces can influence self- and ion diffusion.[22,23] The noticeable reduction in both self- and ion diffusion in bulk simulations when the long-range cutoff is reduced from 12 to 8 Å, observed by Del Buono, Cohen, and Rossky,[22] leads us to attempt no smaller truncation distance than 12 Å. We implement a switched force cutoff for electrostatic interactions and a switched potential cutoff for LJ 12-6 interactions[14] which are applied to groups at 12 Å, slowly turned off from 8 Å. Nonbonded interaction lists are recorded out to 13 Å and are updated at 5–10 fs intervals.

TABLE I. System summary. The channel type, length L, effective radius R, number of water molecules within each channel in the absence of an ion N_{water}, number of water oxygen atoms or molecules on each layer of the wall N_{wall} (multiply by 19 to give the total number in the wall), and water density in the absence of an ion ρ for all dynamics systems are summarized. Atomic refers to the atomic hydrophobic channels, molecular to the hydrophilic channels, and LJ 5-3 to the Lennard-Jones hydrophobic channels.

Type	L (Å)	R (Å)	N_{water}	N_{wall}	ρ (g/cm^3)
Atomic/	51.69	2.1	28	7	0.987
molecular		2.6	43	8	1.009
		3.1	59	9	0.997
		3.6	78	10	0.995
		4.1	100	11	0.995
		4.6	125	12	0.998
		5.1	153	13	1.003
		5.6	183	14	1.001
LJ 5-3	50	2.1	28	···	1.007
		2.6	41	···	0.995
		3.1	57	···	0.996
		3.6	76	···	1.002
		4.1	97	···	0.998
		4.6	121	···	0.999
		5.1	147	···	0.996
		5.6	177	···	1.001
Bulk	25.08	···	528	···	1.000

The water in the channels is sampled from pre-equilibrated bulk coordinates at approximately bulk water density. The density of water within a confined space is difficult to determine accurately since the volume available to the water molecules near the pore surface is not easily defined. One method of determining the correct number of water molecules in each pore would be to ensure that the chemical potential of the channel water is identical to that of bulk. Here we prefer a far simpler procedure which involves redefining the effective volume of the channel. We have defined an effective radius $R=a-1.4$ Å owing to the approximate size of an atom lining the pore being 1.4 Å. However, the spacing of atoms on the wall lattice permits closer packing of water molecules near the surface, thus increasing the effective radius slightly. In studies of water density near a planar hydrophobic wall,[12] it is found that the repulsive core radius of the wall is approximately 2.5 Å. In our studies we find that the LJ 5-3 potentials have repulsive core radii ranging from 2.6 to 2.7 Å. A better effective radius would thus be $R^*=a-2.6+1.4$ Å because water oxygen atom centers approach to within 2.6 Å of the wall atomic centers, and themselves require 1.4 Å to fit their electron clouds. By sampling water molecules from bulk which have oxygen atoms that lie within the radius R, and assuming an effective volume based on radius R^* instead of R, we better approximate the average density of water within the channel. Table I summarizes the system sizes for each of the channels reported in this article.

With oxygen atom centers as close as 1.2 Å from the atomic wall center a, it is not possible to apply the channel wall potential without some prior molding of the system. To do this we have modified the CHARMM program to apply a weak harmonic constraint (8.5 kJ/mol/Å^2) which holds water molecules inside a cylinder whose radius decreases slowly from $R^*=R+0.2$ to $R-1.2$ Å over a period of 10 ps. The strength of this constraint is then increased exponentially to 4.2×10^4 kJ/mol/Å^2 over a further 20 ps. The system then has a ''hard'' wall erected at $R-1.2$ Å. We carry out heating to 300 K over 30 ps and equilibration for a further 90 ps with this hard wall in place. After this time, either the atomic wall or the LJ 5-3 wall potential is introduced with trouble free equilibration of the pure water system where molecules relax and fill the available space.

Prior to the introduction of ions to the channel, equilibration of the water filled system consists of 100–1000 steepest descent minimization steps, 50 ps of heating to 300 K and equilibration, and a further 100 ps of dynamics. An ion is included by placing it at the origin and removing the closest water molecule. After a further 100 steepest descent minimization steps, and 50 ps of equilibration and heating, 2 ns of dynamics is carried out for each system.

For reference purposes, bulk simulations are performed with 528 ST2 water molecules in a periodic box of side 25.08 Å at temperature 300 K. After 110 ps of heating and equilibration, 100 ps of MD is used to determine bulk values of self-diffusion, rotational correlation, hydrogen bonding, and water coordination. A single ion is added to the system, removing water molecules within 2.6 Å of the ion center, leaving 525 ST2 molecules. After 1000 steps of steepest descent minimization and 20 ps of heating and equilibration, 1 ns of trajectory data is used to produce a bulk Na ion diffusion estimate.

C. Analysis

Water structure is analyzed by studying density profiles, radial distribution functions, hydrogen bonding, dipole orientations, and dipole correlations. Density profiles within a cross section of the channel, averaged over the length of the channel and time, are generated with a grid spacing of 0.1 Å. These radial density profiles reveal the ''shell'' structure of channel water. Profiles along the channel axis (z) direction require subtraction of the center of mass translation prior to generation. These profiles reveal the ''layer'' or ''disk'' structure of the channel water.

The water–water and ion–water radial distribution functions (RDFs) are determined via the standard procedure.[24] The hydration number is defined as the number of oxygen atoms falling within the first minimum of the RDF and determined from the integrated RDF. We employ ''directional'' RDFs with respect to a water molecule residing in the outer water shell with cylindrical coordinates (r_1,ϕ_1,z_1). Another water molecule with coordinates (r_2,ϕ_2,z_2) is considered to lie within the same: (i) ''disk'' if $|z_2-z_1|\leqslant\Delta z_{\max}$, (ii) ''shell'' if $|r_2-r_1|\leqslant\Delta r_{\max}$, and (iii) ''sector'' if $r_2|\phi_2-\phi_1|\leqslant\max[r_1,r_2]\Delta\phi_{\max}$. We take $\Delta z_{\max}$ and $\Delta r_{\max}$ to be 1.6 Å (slightly more than half of the mean intermolecular distance), and $\Delta\phi_{\max}$ as approximately half of the mean angular separation of water molecules within the outer water shell. Assuming a circular shell centered at approximately $R-1.2$ Å with intermolecular spacing 3.2 Å we find $\Delta\phi_{\max}\approx0.8/(R-1.2)$. Given these three conditions we define our RDFs: (i) $g_{\text{washer}}(\Delta\phi)$—a water molecule is considered to be within the same ''washer'' if it lies within the same disk, and within the same shell, (ii) $g_{\text{column}}(\Delta z)$—a

water is considered to be in the same ''column'' if it lies within the same shell and the same sector, and (iii) $g_{\mathrm{ray}}(\Delta r)$—a water is considered to reside in the same ''ray'' if it lies within the same disk and the same sector.

Dipole orientations are studied by analyzing the averaged projection of the water dipole $\mu=[\mu_x,\mu_y,\mu_z]$ onto the z axis and onto the radial vector $\mathbf{r}=[x,y]$, leading to the two cosines: $\cos\theta$ and $\cos\phi$, respectively. The average orientation angles θ^{mean} and ϕ^{mean} quoted in the text are found by summing all possible cosine moduli weighted by normalized distribution probabilities, and then taking inverse cosines. When $\theta^{\mathrm{mean}}=0°$ the dipoles are oriented along the z direction, while for 90° they are in the xy plane. In the latter case, $\phi^{\mathrm{mean}}=0°$ corresponds to radially oriented dipoles and 90° to circular ones. Also summarizing the dipole orientations is the net dipole moment of the channel water. The moment about the center of charge is averaged over time for each channel to yield a separate measure of the mean orientation.

Dipole correlations are measured over the same directions as the previously defined RDFs. The dot product of two dipole vectors within the same washer, column, or ray is placed into a bin in the distribution along ϕ, z, and r coordinates, respectively, leading to the functions $C_{\mathrm{washer}}(\Delta\phi)$, $C_{\mathrm{column}}(\Delta z)$, and $C_{\mathrm{ray}}(\Delta r)$. The normalized integral of the product of these distributions with the RDFs produces an average weighted dipole correlation within washers, columns, or rays: $C^{\mathrm{mean}}_{\mathrm{washer}}$, $C^{\mathrm{mean}}_{\mathrm{column}}$, and $C^{\mathrm{mean}}_{\mathrm{ray}}$, respectively.

Hydrogen bonding is measured by the time averaged number of water–water pair interactions with total electrostatic plus LJ 12-6 energy exceeding a minimum attractive interaction. Cutoffs of −8.5, −12.7, or −17.0 kJ/mol have been used near hydrophobic and polar interfaces.[25,12,26] Here we choose an intermediate cutoff value of −12.7 kJ/mol applied in both bulk and channel water simulations.

Water self-diffusion and ion diffusion coefficients are calculated by averaging the mean square fluctuations of oxygen and ion position vectors over the range in time intervals $0.1\leqslant\Delta t\leqslant 10$ ps. Statistical uncertainty is minimized by using an overlapped data procedure.[27] We consider the range 1–10 ps after the initial shoulder, corresponding to inertial motion within the hydration ''cage.'' Before calculating diffusion coefficients, the center of mass motion of the system is subtracted to remove any net momentum associated with the periodic boundary. We break diffusion down into three components, D_z, D_ϕ, and D_r along the axial-z, tangential-ϕ, and the radial-r directions, respectively. In addition, the total nonaxial (transverse) diffusion is given by the quantity D_{xy}. These are given by the fluctuation formulas

$$D_z=\frac{1}{2}\frac{d}{dt}\langle[z(t)-z(0)]^2\rangle,$$

$$D_{xy}=\frac{1}{4}\frac{d}{dt}\langle[x(t)-x(0)]^2+[y(t)-y(0)]^2\rangle,$$

$$D_r=\frac{1}{2}\frac{d}{dt}\langle[r(t)-r(0)]^2\rangle$$

$$D_\phi=\frac{1}{2}\frac{d}{dt}\langle r^2[\phi(t)-\phi(0)]^2\rangle=2D_{xy}-D_r. \tag{6}$$

Because D_r is of little interest in narrow channels it is not considered in this study. The tangential diffusion D_ϕ can be calculated in two ways, of which we prefer the latter in Eq. (6) because of the arbitrariness in the choice of r^2.

Water rotational correlation is determined by analyzing the decay of the dipole autocorrelation. The dipole autocorrelation function is defined as the time and system average of the cosine of the angle $\chi(\Delta t)$ a water dipole at time $t_0+\Delta t$ makes with its dipole at time t_0. A monoexponential decay is assumed and appears to be justified by analysis of the autocorrelation functions. The resulting expression governing the calculation of the inverse rotational correlation time is

$$\tau^{-1}=-\frac{d}{dt}\ln\langle\cos\chi(\Delta t)\rangle, \tag{7}$$

which is valid at large time intervals (Δt). The sampling procedure for this calculation is identical to that used for diffusion.

III. CHANNEL WATER STRUCTURE

We begin with a summary of channel water properties. Water and ion diffusion are determined by the extent of ordering and strength of intermolecular interactions within the channel water. Here we examine the effect of the pore size and type on this structure. Bulk reference values are listed in Table II.

A. Density analysis

Figure 2 shows the water oxygen atom density profiles against distance from the effective wall radius for each wall type and for effective radii $R=2.1$–5.6 Å. The distinct regions of high density near the wall and near the center of the pore have been observed in previous studies.[8,9] The profiles for the atomic and LJ 5-3 hydrophobic walls are very similar. Within hydrophobic channels (solid and dotted curves) one shell of waters exists for $R\leqslant 3.6$ Å while two shells appear for larger pores. A band of water molecules centered at 1.2–1.4 Å from the effective channel radius solvates the pore

TABLE II. Bulk hydration and diffusion. Bulk properties r_{max}, r_{min}, n, n_{HB}, D, and τ^{-1} are the first minima and maxima in the RDF, the first hydration number (nearest neighbors), the number of hydrogen bonds, the diffusion coefficient, and the first-order inverse rotational correlation time constant, respectively. Experimental results are given in square brackets.

Property	Water	Na
r_{max} (Å)	2.82±0.04[2.84][a]	2.34±0.04[2.4][c]
r_{min} (Å)	3.52±0.04	3.12±0.08
n	4.70±0.06[4.4][a]	6.67±0.02[4–6][d]
n_{HB}	2.73±0.05	⋯
D (Å^2/ ps)	0.262±0.006[0.24][b]	0.070±0.007[0.133][e]
τ^{-1} (ps^{-1})	0.084±0.002	⋯

[a]Reference 29.
[b]Reference 18.
[c]Reference 30.
[d]Reference 31.
[e]Reference 32.

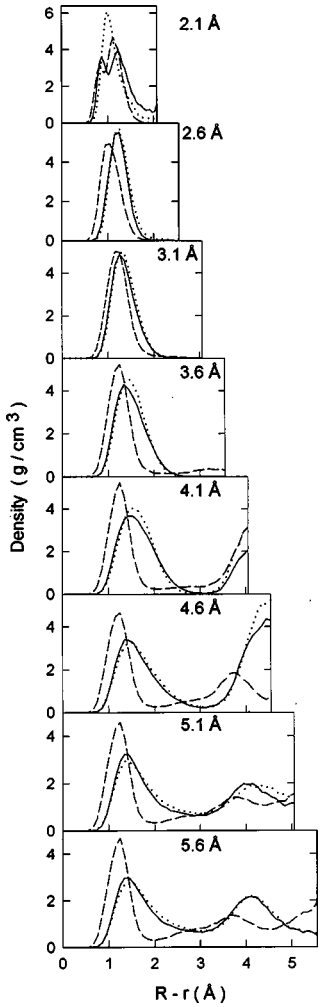

FIG. 2. Water oxygen atom radial density profiles: Density profiles for the atomic hydrophobic (solid curve), LJ hydrophobic (dotted curve), and hydrophilic (dashed curve) channels are compared for effective channel radii 2.1–5.6 Å. All profiles are plotted against the distance from the effective wall of the channel $R-r$. The left-hand vertical axis represents the effective wall while the right hand axis represents the channel axis z. Each graph is labeled with the effective channel radius R.

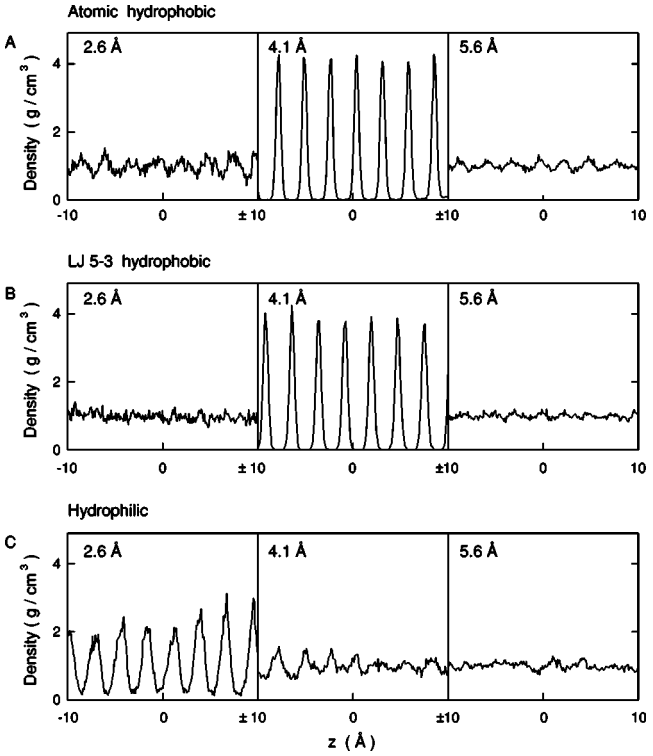

FIG. 3. Water oxygen atom density profiles along channel axis direction: (A) Density profiles for atomic hydrophobic channels of effective radii 2.6 (left-hand panel), 4.1 (central panel), and 5.6 Å (right-hand panel). (B) Density profiles for LJ hydrophobic channels. (C) Density profiles for hydrophilic channels.

lining. As expected, the hydrophobic and hydrophilic channels result in distinct density profiles. Water molecules are able to approach closer to a molecular wall resulting in a more sharply defined density maximum which is shifted toward the wall. Also a third peak in the density profile appears in the larger pores.

Figure 3 displays 20 Å segments of the center of mass corrected density profiles in the z direction for atomic hydrophobic (A), LJ hydrophobic (B), and hydrophilic channels (C) with $R=2.6$, 4.1, and 5.6 Å. In both of the hydrophobic channels, a transition occurs at $R=4.1$ Å (also seen at $R=3.6$ Å), where the water becomes highly structured, and well-defined layers appear. As in the case of Fig. 3, the results for the two hydrophobic channels are very similar, that is, an explicit treatment of the atomic structure of the channel does not have an appreciable effect on water structure. Therefore, in the following structural analysis, the results for the LJ hydrophobic channel will not be shown if they require additional graphs, but will otherwise be included as dotted curves for comparison. In the hydrophilic channels, the water structure exhibits again a markedly different behavior, with only the narrow 2.6 Å channel exhibiting some order in the z direction.

More insights into the structure of water can be obtained from the directional RDFs, which are displayed in Fig. 4 for the atomic hydrophobic (solid curves) and hydrophilic channels (dashed curves). For simplicity, we analyze only the outermost washer, which is the most relevant region since the vast majority of water molecules reside there. For each graph in Fig. 4 corresponding to channel radii 2.1–5.6 Å, the left-hand panels show how water molecules within this washer are distributed in the ϕ direction while the right-hand panels show distributions within columns. The total number of waters in this washer, given at the top of each left-hand panel, equals the integral of this RDF plus one (to account for the molecule in question). Consider first the hydrophobic channels (solid curves). The narrowest 2.1 Å channel represents a near-single file system ($\sim$1.5 water molecules per disk), while the largest 5.6 Å channel contains over eleven water molecules per disk (more than eight in the outer washer alone). For most channel sizes there exists an observable ordered distribution of molecules within each washer. This order is most apparent in the hydrophobic channel of radius 4.1 Å where the five water molecules within the outer washer are arranged in an approximate pentagonal arrangement. That is, two water molecules are at approximately $\pm 72°$ and two at approximately $\pm 144°$, with almost vanishing minima in between. Sample coordinates illustrating this geometry are shown in Fig. 5(A). A similar near-pentagonal

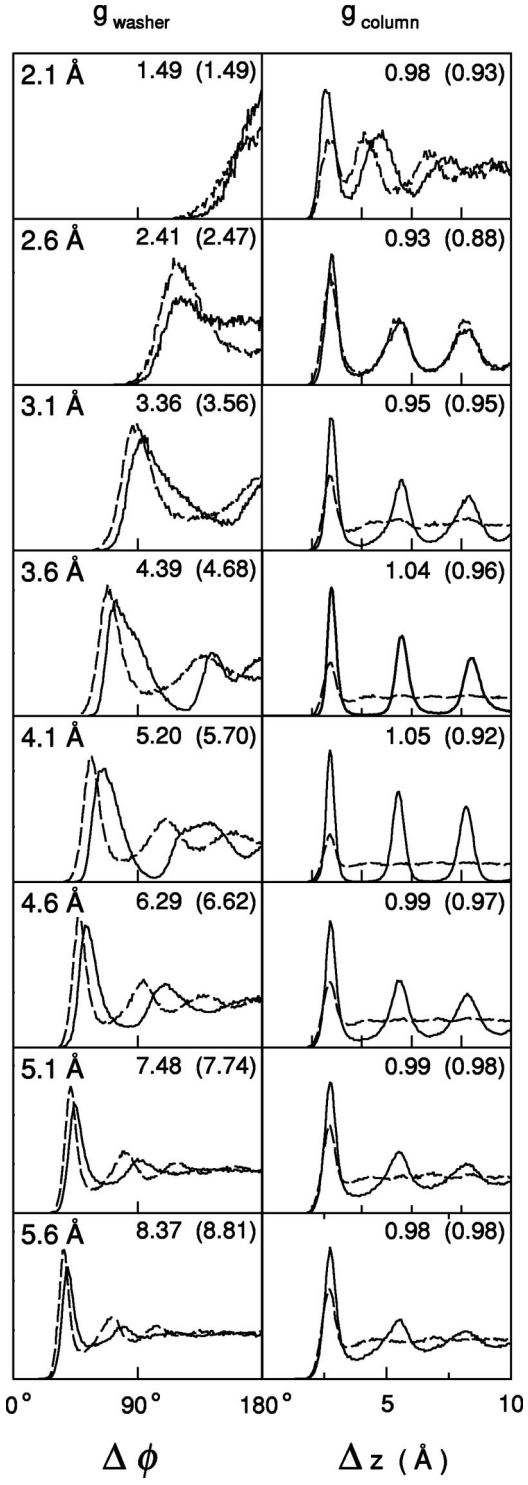

FIG. 4. Water radial distribution functions for the atomic hydrophobic (solid curves) and hydrophilic (dashed curves) channels of radii 2.1–5.6 Å. Each figure has two panels: the left-hand panel is the oxygen atom RDF in the ϕ direction within the outermost washers $g_{\text{washer}}(\Delta\phi)$, while the right-hand panel is the RDF in the z direction within columns in the outermost water shell $g_{\text{column}}(\Delta z)$. Variable axis ranges are used to highlight features of distribution functions. Due to the symmetry of each profile about the origin, distributions include contributions from both sides of the water molecule in question. At the top of the left-hand panels is given the number of water molecules in the outer washer obtained from integrating the washer RDF for the atomic hydrophobic channel, and in brackets the value for the hydrophilic channel. At the top of the right-hand panels is given the number of water molecules within the column per 3.14 Å obtained from integrating the column RDF.

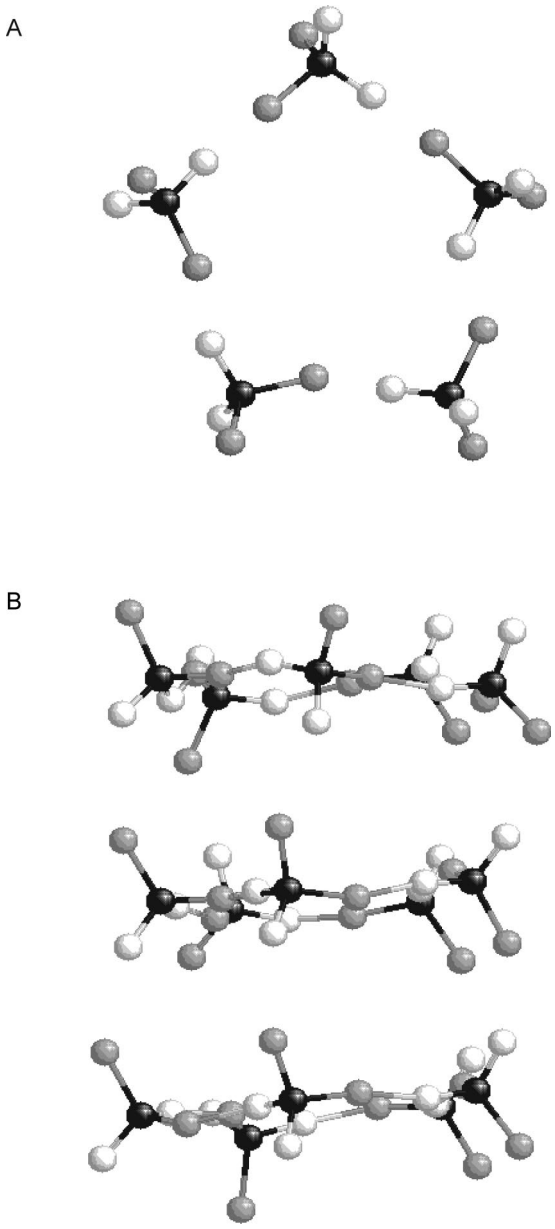

FIG. 5. Pentagonal arrangement of waters: (A) A sample disk of waters taken at random from the end of the simulation of an atomic hydrophobic channel with radius 4.1 Å. (B) Three disks of waters as viewed along the x axis. Oxygen atoms are black, hydrogens gray, and lone pairs white.

geometry is also observed in the 3.6 Å hydrophobic channel.

The RDFs within columns (right-hand panels of Fig. 4) have density maxima diminishing in size with distance which is due to the restricted window in the ϕ direction. Again the level of ordering becomes most prominent for the moderate sized ($R=3.6-4.1$ Å) hydrophobic channels. The mean number of waters in a column per 3.14 Å (the approximate mean intermolecular distance), averaged over the range $|\Delta z|\leqslant 10$ Å, is shown at the top of each graph on the right-hand panel. This value is a maximum for the moderate hydrophobic pore sizes, again reflecting the extent of ordering in those channels and the strength of interactions between neighboring water molecules in the axial direction. Figure 5(B) shows a random sample containing three disks of water molecules within the 4.1 Å atomic hydrophobic channel. The

distinct layering and the hydrogen bonding within columns of water molecules are obvious in this illustration.

The hydrophilic channel RDFs (dashed curves in Fig. 4) show a different dependence on channel radius. The structure of water within the outer washers (left-hand panels) remains well defined, but the density minima at radii 3.6–4.1 Å do not drop to near zero as they do in the hydrophobic channels. In other words, no anomalous stability is observed in the hydrophilic channels. Within columns (right-hand panels) only the narrow 2.6 Å channel, and to a lesser extent the 2.1 Å channel, exhibit a high level of ordering away from nearest-neighbor disks. Therefore, within hydrophilic channels there exists strong interaction between adjacent disks, but weak interaction between distant disks.

B. Energy and hydrogen bonding

Figure 6(A) shows the variation in the average total system energy per water molecule. Within both hydrophobic channels (solid and dotted curves, closed circles) the energy decreases to a minimum for $R=3.6-4.1$ Å and then increases and levels off as radius becomes large. This feature is not observed within the hydrophilic channels (dashed curve, open circles), where the energy stays nearly constant across the range of radii. The minimum in the energy at moderate hydrophobic channel radii is associated with increased attractive interactions of neighboring molecules. The extent of hydrogen bonding is maximized at moderate radii [Fig. 6(B)] where greater than bulk levels are observed. Figure 6(C) reveals that the number of nearest-neighbor molecules levels off for small radii and only begins to increase for $R>3.6$ Å. Figure 2 shows that this corresponds to the onset of a second shell of high water density. For $R\leqslant 3.6$ Å the channel water cannot achieve optimum packing and will suffer from elevated free energy.

Within the hydrophilic channels there are no large variations in the energy, number of hydrogen bonds, or the number of nearest neighbors with the channel radius. Nearest neighbors and hydrogen bonds have been raised in comparison to the hydrophobic channels as a result of the majority of channel waters having access to the molecular wall. If we discount the hydrogen bonds involving wall water molecules in the hydrophilic channels, then a significant reduction in hydrogen bonds is observed [dash-dot-dot curve of Fig. 6(B)], as seen in previous studies of polar surfaces.[26] When the wall water molecules are excluded, the mean number of hydrogen bonds per channel water molecule is significantly lower than that for the corresponding hydrophobic channels. Thus water molecules sacrifice water–water hydrogen bonds for water–wall hydrogen bonds. This strong interaction between channel waters and fixed wall molecules is likely to result in a reduced average self-diffusion.

C. Dipole distributions and the hydrophobic anomaly

Perhaps the most obvious difference between hydrophobic and hydrophilic channels comes from the average water dipole orientation distributions. In Figs. 7(A), 7(B), and 7(C), we show the $\cos\theta$ (left-hand panels) and $\cos\phi$ (right-hand panels) distributions for the $R=2.6$, 4.1, and 5.6 Å

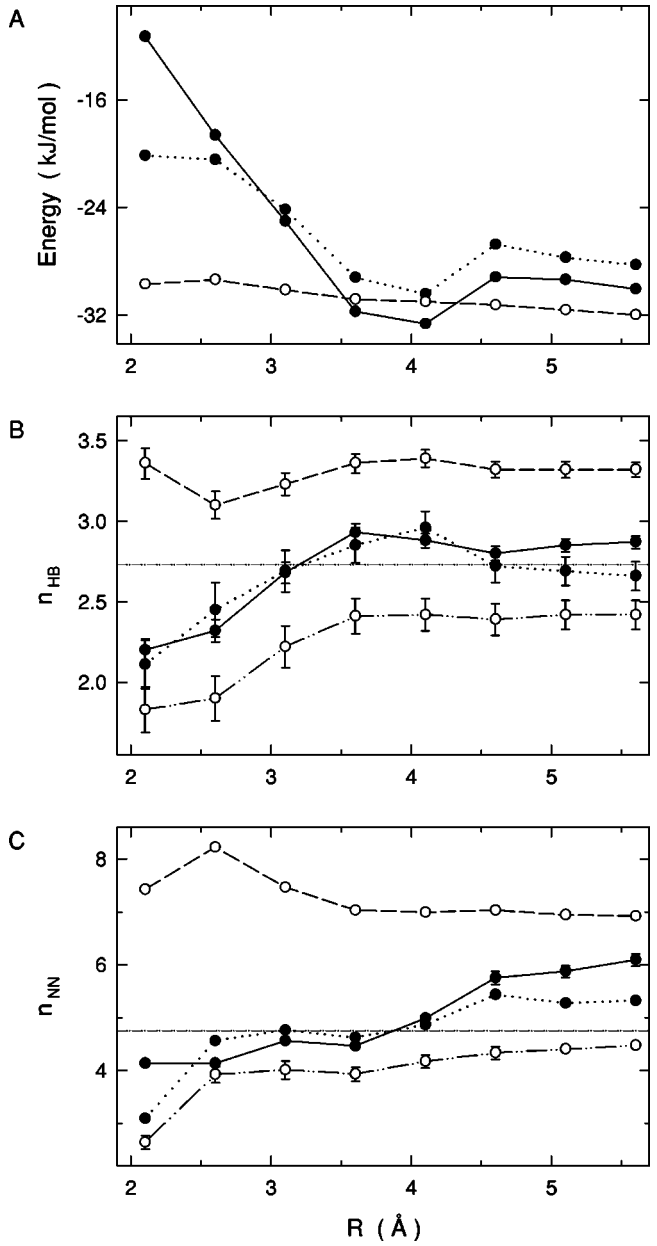

FIG. 6. The effect of pore radius on the total system energy per water molecule (A), the number of hydrogen bonds per water molecule n_{HB} (B), and the number of nearest neighbors n_{NN} (C) for the atomic hydrophobic (solid curves, filled circles), LJ hydrophobic (dotted curves, filled circles), and the hydrophilic channels (dashed curves, open circles). The number of hydrogen bonds and nearest neighbors in hydrophilic channels when channel wall molecules are excluded are drawn as dash-dot-dot curves (open circles). Error bars are one standard error of means for energy values, while those for n_{HB} and n_{NN} are $\pm$ one standard deviation.

channels, respectively. In the hydrophobic channels (solid and dotted curves), water molecules have a definite preference to point either up or down the channel axes. This trend is very clear in the narrow channels but becomes less well defined with growing radius as secondary shells of water appear. Most distributions possess symmetry about the origin and result in zero net dipole moment (to within statistical uncertainty). Exceptions occur for the narrow $R=2.1-2.6$ Å channels where there is only one maximum in their $\cos\theta$ distributions, that is, the molecular dipoles all prefer to point

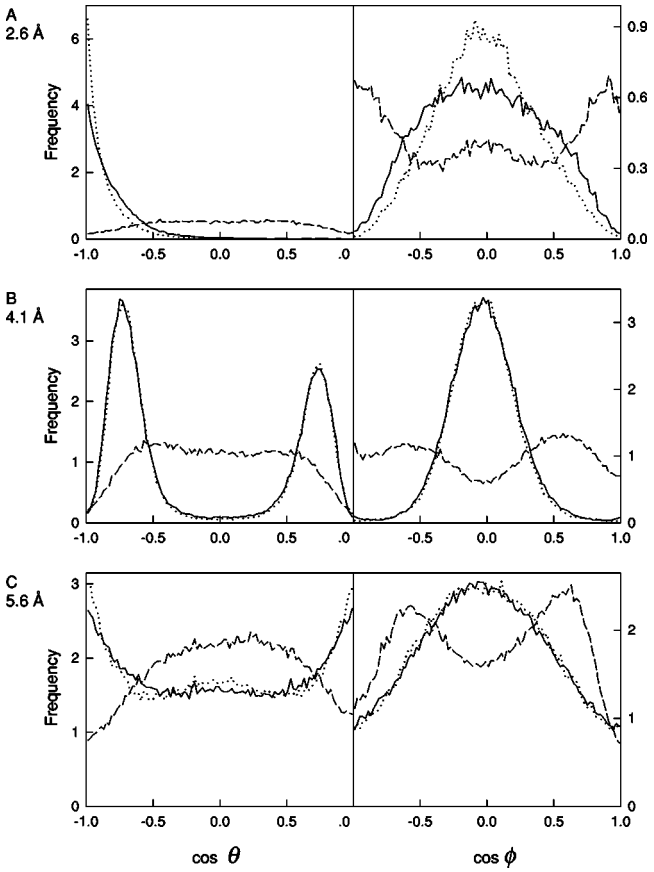

FIG. 7. Water dipole orientation distributions for channels of effective radius 2.6 (A), 4.1 (B) and 5.6 Å (C): The left-hand panels show the average projections of μ onto the z axis ($\cos\theta$) for atomic hydrophobic (solid curve), LJ hydrophobic (dotted curve), and hydrophilic (dashed curve), channels. The right-hand panels show the projections onto the radial vector $\mathbf{r}$ ($\cos\phi$).

down the channel axis. This leads to a rather large net dipole moment per water molecule, namely, 2.04 ± 0.06 D for the 2.1 Å channel and 1.84 ± 0.14 D for the 2.6 Å channel (cf. ST2 dipole moment is 2.35 D). There is also a small asymmetry in the distributions of the moderate size 3.6–4.1 Å channels [as seen in Fig. 7(B)], leading to relatively small net dipole moments of 0.16 ± 0.09 and 0.26 ± 0.06 D, respectively. Within the hydrophilic channels (dashed curves of Fig. 7), the water dipoles prefer to lie in the xy plane rather than run up or down the channel axis, and orient themselves more toward the channel wall (maxima in $\cos\phi$ distribution away from zero). Net dipole moments are zero for all hydrophilic channels.

This contrast in orientation is expected to have some influence on water and ion diffusion within these channels. For example, a charge or dipole (ion or water molecule) attempting to pass alongside a line of dipoles arranged head to tail will be impeded less than if it were to attempt to pass alongside a line of dipoles oriented perpendicular to the line. Calculation of potential barriers indicates a maximum height of about 12–15 kJ/mol along the pore lining of the hydrophobic channels, whereas barrier heights of as large as 150 kJ/mol are observed within the large hydrophilic channels. While the presence of an ion would alter the local orientation of water dipoles, thus reducing these barriers, there would still remain some effect of the natural dipole orientations caused by confinement.

We make some simple observations regarding the geometry and dipole orientations of water molecules in hydrophobic channels. The number of water molecules in a single washer near the channel wall, provided in the left-hand panels of Fig. 4, reveals the average water geometry within disks. Interpolating these numbers we see that three waters would be arranged in a triangle (at 60° between neighbors) for a radius $R=2.9$ Å, four waters arranged in a square (at 90°) for $R=3.4$ Å, five waters arranged in a pentagon (at 108°) for $R=4.0$ Å, six waters in a hexagon (at 120°) for $R=4.5$ Å, and so on. The angle between hydrogen, oxygen, and lone pair atoms within an ST2 water molecule is constant at 109.5°. Thus, if a water molecule attempts to form hydrogen bonds with both of its nearest neighbors within a washer, then it can do so most effectively for a pentagonal arrangement which occurs at a channel radius of approximately 4 Å. If one hydrogen and one lone pair were to lie on the xy plane then the water dipole must have a θ value of 45°. Our orientation studies have revealed a preference for dipoles to run around each washer ($\phi^{\text{mean}}=78°$), elevated out of the plane such that $\theta^{\text{mean}}=46°$. Therefore, moderate size hydrophobic channels exhibit near optimal configurations for strong hydrogen bonding. This situation is observed in any randomly chosen sample disk of waters [e.g., Fig. 5(A)], and offers an explanation for the high level of ordering within disks, and consequently between disks, in these moderate channel sizes. Because there are an odd number of water molecules within the disk, and this optimal hydrogen–lone pair configuration requires that the dipole vector be lifted out of the plane by approximately 45°, it is unlikely that a zero net dipole within each disk will occur. In Fig. 5(B) we observe 3 water dipoles in the pentagon directed downwards while 2 are directed up the channel axis. This pattern is repeated throughout the entire cylinder. This explains the small asymmetry in the dipole distribution of Fig. 7(B) and the nonzero dipole moment. Figure 5(B) also reveals hydrogen bonding between disks of water molecules, which is a consequence of the dipole orientations.

An optimal-configuration phenomenon is not observed in the hydrophilic channels as a result of the smaller preferred angle ϕ^{mean} of under 60° which can be attributed to the strong interactions with the molecular wall. We remark that a similarly anomalous stability is observed near $R=4$ Å in pores with exponentially repulsive walls using the SPC/E water model.[9] Therefore, this phenomenon is not a consequence of the ST2 charge distribution or the wall type used, but appears to be a generic feature of water confined in a hydrophobic cylinder with radius $R\approx4$ Å.

D. A measure of structure: Dipole correlation

We now briefly examine dipole correlation in an attempt to understand how neighboring molecules arrange themselves so as to, with the exception of the very narrow hydrophobic channels, produce near-symmetric dipole distributions, thus minimizing the net dipole moment and the electrostatic energy. They are also a very good measure of the extent of ordering within the system. The RDF weighted

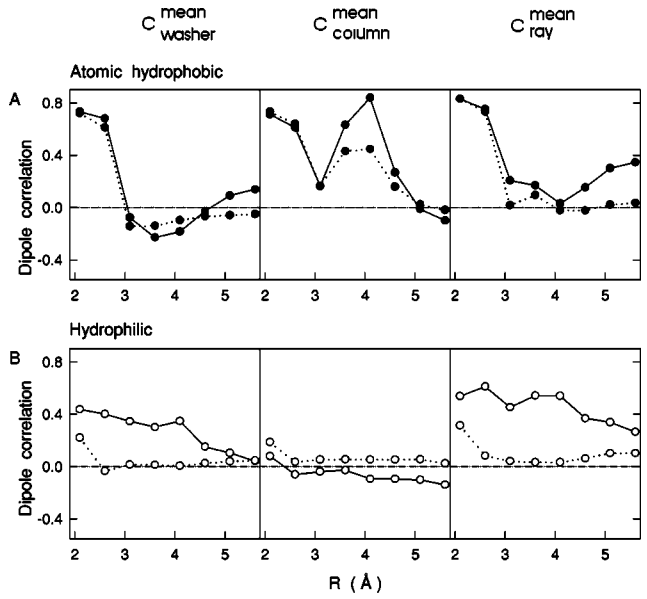

FIG. 8. Effect of pore size on weighted average dipole correlations: A and B correspond to the atomic hydrophobic (filled circles) and hydrophilic (open circles) channels, respectively. Weighted averages over washers $C_{\text{washer}}^{\text{mean}}$ (left-hand panels), columns $C_{\text{column}}^{\text{mean}}$ (central panels, considering the range ± 10 Å), and rays $C_{\text{ray}}^{\text{mean}}$ (right-hand panels), of the dipole correlation are drawn as solid curves. Weighted averages of z components of dipole correlation are drawn as dotted curves.

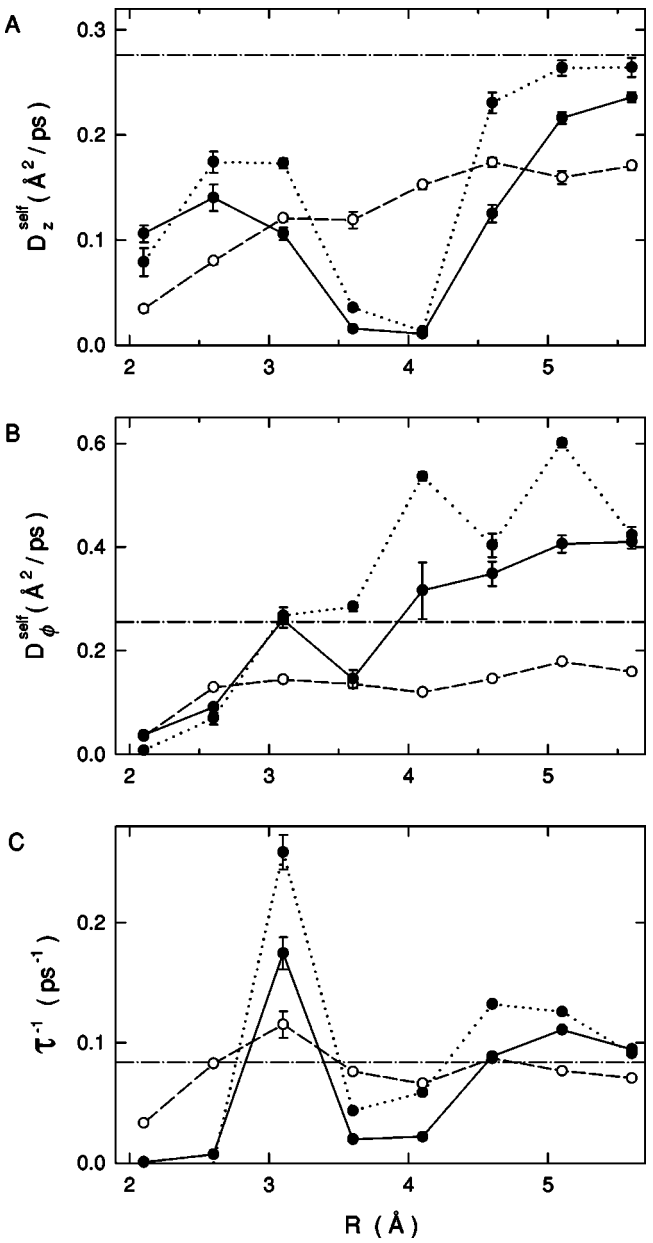

FIG. 9. Self diffusion and rotational correlation: (A) axial self-diffusion D_z^{self}, (B) tangential self-diffusion D_ϕ^{self}, and (C) first-order inverse rotational correlation time constant τ^{-1} for the atomic hydrophobic (solid curves, filled circles), LJ hydrophobic (dotted curve, filled circles) and hydrophilic (dashed curve, open circles) channels are compared. The horizontal dash-dot lines (no symbols) are the bulk reference values from Table II. Error bars are one standard error of means.

average correlations within washers, columns and rays for atomic hydrophobic and hydrophilic channels are provided in Figs. 8(A) and 8(B), respectively. Before discussing the complex features of the plots for the hydrophobic channels we remark on the hydrophilic pores [Fig. 8(B)]. Within the hydrophilic pores, dipoles are always positively correlated within both washers and rays while there is little correlation in columns. This can be attributed to the strong interactions with the molecular wall. There is negligible correlation of dipole z components [dotted curves of Fig. 8(B)] in any direction and this explains the near-zero net axial dipole moments within all hydrophilic channels. Also, in related analysis, we observe a strong positive correlation between water molecules bound in the hydrophilic wall and those inside the channel within the same ray. This is not surprising given the general positive correlation between shells ($C_{\text{ray}}^{\text{mean}}$) within the channels, and the extent of hydrogen bonding between channel and wall water molecules.

In the hydrophobic channels [Fig. 8(A)] with small pore radii there is a strong positive correlation between water dipoles in washers, columns, and rays (total and z-dipole components) which explains the strong net dipole of the channel contents. This behavior is expected due to the small dimensions of the pore and the near single-file nature of the water. In all directions, this correlation drops to small values for $R=3.1$ Å, where we would anticipate large diffusion and short rotational correlation times. At moderate sizes ($R=3.6$–4.1 Å), the correlation within each washer increases (negative) and drastically increases within columns (positive). Therefore, in the medium size hydrophobic channels, dipoles are correlated such that cancellation occurs within each disk and not from adjacent layers, in agreement with the analysis of dynamics coordinates, such as shown in Fig. 5. This is the reverse of what is seen in the corresponding hydrophilic channel. The mean correlation of nearly unity [see the central panel of Fig. 8(A)] is indicative of the rigid structure seen in Fig. 5(A). The maxima in correlation within both washers and columns at radii 3.6–4.1 Å explain the highly ordered configurations, and are expected to result in decreased translational and rotational diffusion. For pores larger than 4.1 Å, correlation is again reduced within washers and columns, becoming more positive in washers and rays, but likely to settle to zero in the bulk limit.

IV. WATER SELF-DIFFUSION

Figure 9 shows self-diffusion and first-order inverse rotational correlation times for each channel type against radius. As anticipated, axial self-diffusion [Fig. 9(A)] within hydrophobic channels experiences a dramatic fall at moderate channel sizes (3.6–4.1 Å), which is associated with anomalous stability. Diffusion has effectively been eliminated at these radii, falling to as low as 4% of bulk. For smaller hydrophobic channels, D_z rises to about half the bulk value for the hydrophobic channels at $R=2.6$ Å. Because the narrowest channel (2.1 Å) is not small enough so that the water forms a true single file system, self-diffusion does not experience the significant attenuation associated with single file diffusion.[3] As channel radius is increased past 4.1 Å, D_z rises, asymptoting at the bulk diffusion level. The atomic and LJ 5-3 potentials give similar self-diffusion results over this range in channel size; the small deviations owing to a small increase in layering associated with the corrugated wall. In hydrophilic channels, D_z increases steadily from 13% to 66% of bulk diffusion. The relatively smooth increase in hydrophilic D_z was anticipated based on structural analysis. There is a reduction in axial self-diffusion for hydrophilic channels with respect to the hydrophobic channels for small and large pores that can be attributed to the preferred dipole orientations and hydrogen bonding with fixed wall molecules.

If we ignore the anomalous lack of axial diffusion for moderate size hydrophobic channels, there is a general upward trend with radius that can be explained in terms of a general decrease in channel water structure with R. As R increases, the separation of water molecules into well-defined and correlated regions becomes less apparent and water molecules become more free to translate in the axial direction. Simulations with an exponentially repulsive channel wall and the SPC/E water model[9] also produce this general trend, and anomalous diffusion at $R\approx 4$ Å, though the reduction in self-diffusion is not as pronounced (only ≈40% reduction). In parallel studies with the ST2 water model where a strong harmonic confining wall potential is employed, we have observed a similar anomaly for $R=3.6-4.1$ Å, with the axial self-diffusion dropping to ≈23% of bulk. Thus the small attractive component of the wall potential appears to add an extra stability to water structure at these radii, suppressing axial diffusion further.

Although transverse motions of water molecules are not likely to have the impact on axial ion diffusion that axial water motions have, it is of some interest how free molecules are to move perpendicular to the pore axis, and how this motion is dependent on pore size and constitution. In all but the wide channels ($R\geqslant 4.6$ Å), transverse self-diffusion can be considered to be almost completely in the ϕ direction (water molecules moving in circles). Results for D_ϕ are plotted in Fig. 9(B). Equation (6) shows that D_ϕ has an r^2 dependence, and since most water molecules reside in the outer shell near the channel wall, we expect D_ϕ to increase as the channel radius grows. This general behavior is obvious in both hydrophobic channel types. A significant decrease in D_ϕ is not obvious for our 3.6–4.1 Å hydrophobic pores. The anomalously high levels of dipole correlation in the 3.6–4.1 Å hydrophobic channels have most strongly affected axial diffusion and have had minimal influence on transverse components. Since we have observed well-defined columns of water molecules (Fig. 4) and strong positive dipole correlation within columns [Fig. 8(A)], transverse diffusion for 3.6–4.1 Å hydrophobic channels must involve a considerable amount of collective motion of disks, indicating a lack of wall friction. Analysis of water trajectories has shown that almost all water molecules rotate around the z axis at the same time within these moderate-sized hydrophobic channels. In contrast, rotations around the z axis are far less cooperative in the hydrophilic channels, and are reduced owing to the preferred dipole directions and hydrogen bonding with wall molecules.

Consider next the inverse rotational correlation of water molecules [Fig. 9(C)]. Both hydrophobic channels experience a gain in rotational freedom at radius 3.1 Å, as well as large radii. In fact, the inverse rotational correlation time constant exceeds the bulk value for $R=3.1$ and 4.6–5.6 Å. Examination of Fig. 8 shows that there is least dipole correlation within the channels at these radii. The obvious drop in rotational freedom at 3.6–4.1 Å corresponds to the highly correlated, highly ordered systems.

V. ION STRUCTURE

We report our findings regarding ion positions and solvation within these channels before discussing ion diffusion estimates. In Fig. 10 we compare ion radial probability distributions (solid curves for atomic hydrophobic channels in the left-hand panel, dashed curves for hydrophilic channels in the right-hand panel) with the density profiles for water (dotted curves). In hydrophobic channels, the distance of the ion from the channel axis remains under 0.7 Å for effective radii 2.1–3.6 Å (ion between water shell and channel axis). With increasing radii a second water shell develops near the center, and the ion moves further away from the axis. These distributions are qualitatively similar to those found with exponentially repulsive cylinders.[9] In all channel sizes, the ion prefers to reside in regions of minimum water density, hydrated by neighboring shells. There is, however, a tendency for the ion in the narrowest 2.1 Å channel to reside within the band of high water density (near single-file system). For the larger pores the ion probability distribution is spread more evenly over the interior of the channel as a result of the more uniform water distribution.

Within hydrophilic channels (right-hand panels) the ion prefers to dwell near the channel wall lining, except for the largest channel ($R=5.6$ Å) where it tends to reside between water shells. In $2.1\leqslant R\leqslant 4.1$ Å channels, the ion is about 0.3 Å away from the effective wall at $r=R$. Within larger channels ($R=4.6-5.1$ Å), the ion moves outwards and sits almost on the wall ($r=R-0.05$ Å). We observe the ion existing between layers of the molecular lattice. In this position, the ion-nearest wall oxygen distance is 2.35 Å, which corresponds to the position of the first hydration maximum in the bulk Na ion RDF (Table II). Thus, for these two large hydrophilic channels, the curvature of the cylinder is such that the wall molecules provide an optimal hydration for the ion, so it prefers to stay very close to the pore lining.

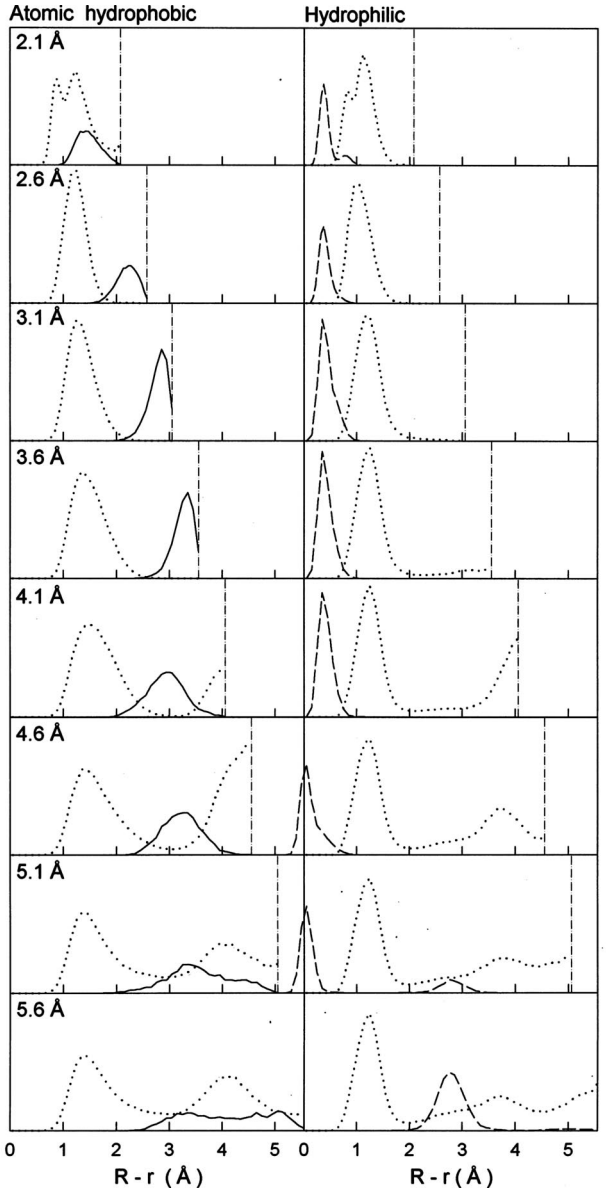

FIG. 10. Ion probability distributions: The left-hand panels show the ion probability distribution (solid curves), against $R-r$, for the atomic hydrophobic channels of radii 2.1–5.6 Å. The average number of ions within a shell of thickness 0.1 Å in the radial direction is plotted. The corresponding water density profiles are drawn as dotted curves. The right-hand panels show the ion distributions for the hydrophilic channels (dashed curves) with corresponding water density profiles superimposed (dotted curves). The axis range for the water density is 0–5.75 g/cm^3 for all graphs. The axis range for ion numbers is 0–0.35. Vertical dash-dot lines represent the channel axis in each figure.

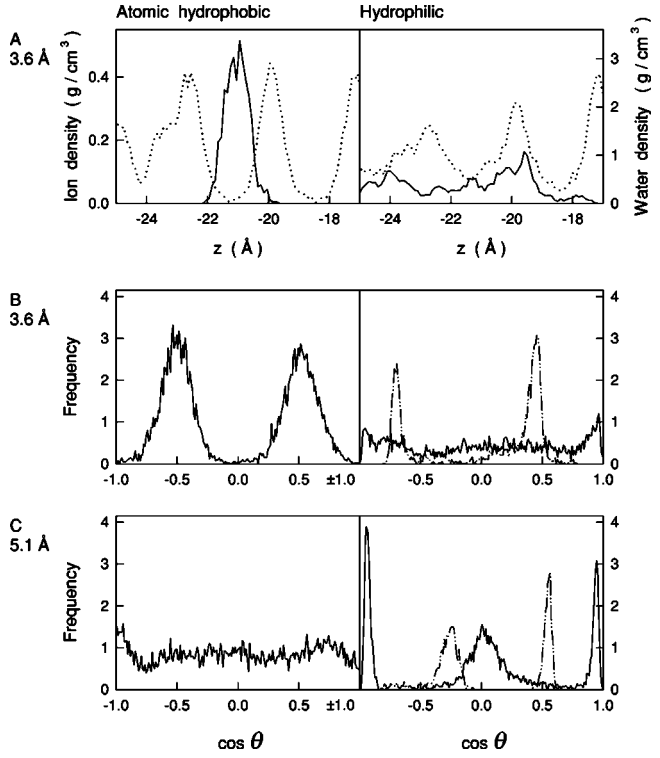

FIG. 11. (A) Ion z profiles: The ion and water densities within an 8 Å segment of the atomic hydrophobic (left-hand panel) and hydrophilic (right-hand panel) channels of radius 3.6 Å are shown as solid and dotted curves, respectively. (B) Hydration shell distributions for $R=3.6$ Å channels: The distribution of water oxygen atoms within the first hydration shell around the ion, as measured by the angle θ the ion–oxygen vector makes with the z axis, is shown. The dash-dot-dot curve in the right-hand panel is the contribution from the hydrophilic channel wall molecules. (C) Same as (B) but for $R=5.1$ Å channels.

We also see localization of ion density along the channel axis direction as illustrated for the hydrophobic 3.6 Å channel in Fig. 11(A). We note that localization is most evident in the 3.6 and 4.1 Å hydrophobic channels and either pore size could be chosen to illustrate this effect. The left-hand panel of Fig. 11(A) shows how the ion resides between water disks in the hydrophobic channel. In contrast, there is a fairly uniform distribution of the ion in the hydrophilic channel (the right-hand panel). The ion–water geometry is further quantified in Fig. 11(B), which shows the angle θ the ion–oxygen vector makes with the channel axis. As a result of the ion residing between disks and between shells of waters within hydrophobic channels, the θ distribution of water molecules within the first hydration shell of the ion exhibits no 0, 90°, or 180° components [left-hand panel of Fig. 11(B)]. The fact that the water molecules within the hydrophobic channel are unable to diffuse freely for $R=3.6$ Å [Fig. 9(A)] suggests that the ion could move within these density troughs with little friction from neighboring water molecules. The situation in the hydrophilic channel of the same radius [the right-hand panel of Fig. 11(B)] is very different. Although the ion prefers to reside within a plane between the layers of the molecular wall (dash-dot-dot curve), a fairly uniform distribution of channel waters around the ion exists (solid curve). Now consider the larger 5.1 Å channels [Fig. 11(C)] in which we have observed a strong attachment between the ion and the molecular wall (Fig. 10). There is a complete reversal in the water distribution, which becomes uniform in the hydrophobic channel [the left-hand panel of Fig. 11(C)], and ordered in the hydrophilic one [the right-hand panel of Fig. 11(C)]. Inspection of the ion hydration geometry in the hydrophilic channel reveals fixed wall waters in the layer above the ion (near $\cos\theta=0.5$), and in the layer below the ion (near $\cos\theta=-0.3$). The free water molecules (solid curve) fill the spaces around the ion with clear preferences for $\theta=0°$, 90°, and 180° positions. The Na ion is therefore strongly solvated by the molecular wall for $R=4.6-5.1$ Å, and is surrounded

by water molecules in axial and transverse directions. These factors are likely to cause reduced ion diffusion for these hydrophilic channels. The absence of concentrated hydration waters in the axial and transverse directions in the larger hydrophobic channel is expected to lead to high levels of ion diffusion.

The first hydration numbers, obtained from Na^+ ion RDFs, together with the ion electrostatic potential energy calculations, reveal that the hydrophobic channels have difficulty permitting complete solvation of the ion for small pore radius. For very narrow channels the first coordination number is reduced to as little as 4, while it asymptotes at a little over the bulk value at large radius. The first hydration number of the ion within hydrophilic channels, on the other hand, remains approximately constant at the bulk value for all R. Inside all hydrophilic channels with $R \leqslant 5.1$ Å, approximately half of the ion's solvating molecules belong to the channel wall which should tend to lower ion diffusion coefficients relative to the hydrophobic channels. At radii $R = 4.6–5.1$ Å this number is raised slightly, which, combined with the propensity for the ion to be partially embedded in the wall, will result in reduced ion mobility. The ion-wall coordination contribution then drops to zero for the largest pore radius $R = 5.6$ Å corresponding to the ion being released from the channel wall, with unfavorable planarlike geometry, toward the center of the channel.

VI. Na ION DIFFUSION

Because there are obvious ranges in channel size where water molecules are relatively free to move and rotate, and ranges where there is little translation or rotation of water molecules, one could naively expect that an ion would also experience large variations in its diffusion. Figure 12(A) displays the z component of the Na ion diffusion. We expect a general upward trend in axial ion diffusion with pore size because of the increase in axial water diffusion associated with reduced ordering and correlation of molecules as channel radius increases. Within hydrophobic channels (solid and dotted curves) there is a gentle increase in D_z with pore radius, experiencing only small fluctuations. In atomic hydrophobic channels the ion diffusion D_z ranges from 10% to 64% of bulk while in LJ 5-3 channels the Na diffusion ranges from 18%–81% of bulk diffusion. It is clear that the influence of the corrugated channel wall has reduced axial ion diffusion for the atomic hydrophobic channels relative to the structureless LJ hydrophobic channels. The anomalously low diffusion of water at moderate sizes is not evident in the ion diffusion. This feature can also be observed in channels with exponentially repulsive walls.[9] Consider, for example, the $R = 3.6–4.1$ Å hydrophobic channels where axial self diffusion almost vanishes [Fig. 9(A)], but where Na diffusion is only marginally reduced. Since a hydrated ion would not move if the water cannot move, this means that the ion must be able to diffuse within zones of low water density, exchanging solvation waters as it moves.

Within hydrophilic channels [the dashed curve of Fig. 12(A)] D_z ranges from 12%–44% of bulk. There is a fairly large drop in D_z at the larger 4.6–5.1 Å pore radii corresponding to the strong attachment of the ion to the molecular wall, as demonstrated in Fig. 10 and by calculation of ion coordination and electrostatic potentials. In addition, there is a significant axial ion coordination [$\theta = 0$ and 180°; Fig. 11(C)], which further attenuates axial diffusion.

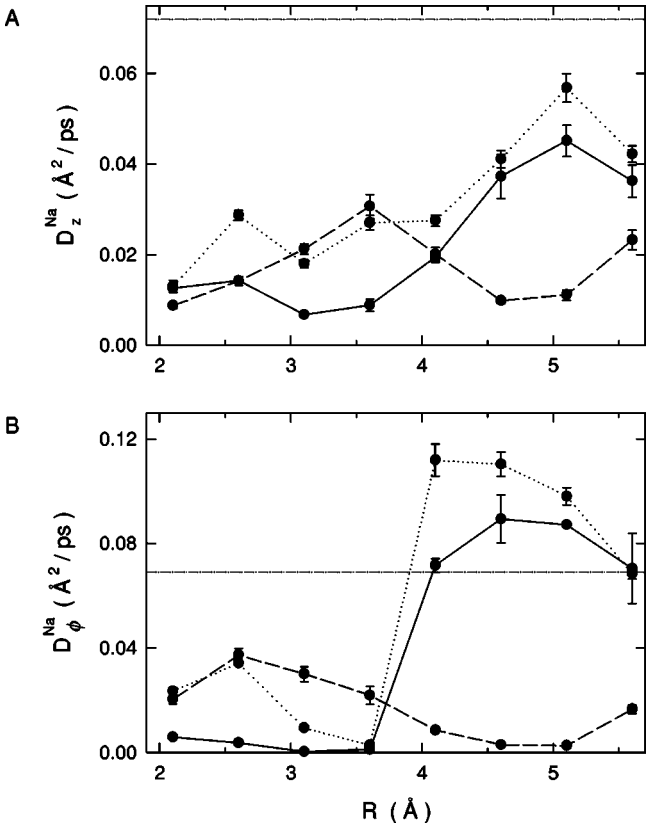

FIG. 12. Sodium ion diffusion: (A) D_z^{Na} and (B) D_ϕ^{Na} for atomic hydrophobic (solid curve, filled circles), LJ hydrophobic (dotted curve, filled circles) and hydrophilic (dashed curve, open circles) channels are compared to the bulk value (horizontal dash-dot line, open circles). Error bars are one standard error of means.

Tangential Na diffusion (D_ϕ) exhibits a clear size dependency. Within $R \leqslant 3.6$ Å hydrophobic channels the ion resides closest to the channel axis at about $r = 0.3–0.5$ Å (cf. Fig. 10). Because the shell of hydrating waters has a well-defined peak (Fig. 10), the ion has little freedom to move away from its optimum radial position and is restricted to move around the channel axis. When the ion resides very close to the axis it cannot diffuse in this direction either, thus the attenuated tangential diffusion for small hydrophobic channels seen in Fig. 12(B) (solid and dotted curves). When the ion is released from the pore center ($R \geqslant 4.1$ Å), transverse diffusion rapidly increases, with D_ϕ reaching the bulk level. Within hydrophilic channels [the dashed curve of Fig. 12(B)] the ϕ component of ion diffusion is further diminished. For $R < 5.6$ Å, approximately half of hydration waters are taken from the channel wall. This, combined with much transverse coordination and reduced self-diffusion explains the reduced ϕ component of ion diffusion within all hydrophilic channels.

VII. SUMMARY AND CONCLUSION

In this paper we have used MD simulations to investigate the influence of pore constitution and size on water and

ion structure and diffusion. In hydrophobic pores, water structure and self-diffusion exhibit a dramatic dependence on the pore size. The packing of water molecules into medium size hydrophobic pores leads to near optimum hydrogen bonded networks such that the system becomes anomalously stable leading to near complete attenuation of water self-diffusion. This enhanced stability is not seen to the same extent in studies with repulsive cylinders,[9] which suggests that it is the attractive component of the atomic wall that leads to additional structure within the channel. Indeed our simulations repeated with a confining hard wall and the ST2 water model resulted in less stable water structure confirming this observation. Although the ST2 model exhibits explicit lone-pair ''atoms,'' it is unlikely that the extent of stability within these pores can be explained by exaggerated charge distributions around the water molecules. Because of the different preferred dipole orientations within the hydrophilic pores, no anomalous stability is observed.

The atomic hydrophobic channels are well represented by a one-dimensional potential function. The LJ 5-3 function gives a very good reproduction of structural and dynamical properties of water and ions for all channel sizes. The significant decrease in simulation times with the use of this function makes it very useful for many applications involving narrow hydrophobic pores. With the use of the LJ 5-3 potential, computation times are reduced by a factor of 2–4. This factor would be increased if the ratio of the number of wall to water atoms were to be increased. The use of this potential function in MD studies of ion selectivity, structure, and diffusion within the potassium channel[28] made it possible to simulate for long enough periods to resolve small ion energy barrier differences, and produce ion diffusion profiles. If the entire protein of the channel were to have been included, these simulations would not have been possible.

Ions are found to reside between shells of water molecules within atomic and LJ hydrophobic pores. The presence of just one water shell for narrow channels ($R \leqslant 3.6$ Å) results in the ion residing very close to the channel axis. In contrast, ions prefer to lie close to the pore lining in a hydrophilic channel for all radii except the largest 5.6 Å channel. The polarizable channel lining provides an energetically favorable environment for the ion up to $R=5.1$ Å. Above this radius the wall lattice approaches a planarlike geometry and the ion is released from the channel wall. As a result of the uniform packing of wall molecules and the size of the Na ion, wall molecules fit perfectly into the ion's hydration shell for pore radii 4.6–5.1 Å where the ion sits against the wall lining. This phenomenon is dependent on the wall-lattice geometry and may occur at a different pore radius for a real hydrophilic pore. The ability of narrow hydrophilic channel walls to attract the Na ion has been observed in gramicidin A[5] and in a model potassium channel.[28]

Despite the large variations in axial self-diffusion with hydrophobic channel radius, axial ion diffusion experiences a fairly smooth growth with pore size. We have observed ions residing between well-defined shells and disks of waters. Although the water is almost incapable of translation, the ion maintains a relatively high level of axial diffusion due to the absence of obstacles in its path. It appears that when the channel water becomes highly stable, the ion moves in troughs of water density where it can remain solvated with only small motions and rotations of water molecules. Within hydrophilic channels these troughs are not so well defined. As a result of water molecules surrounding the ion in axial and transverse directions, ion diffusion becomes subject to levels of self-diffusion within the hydrophilic channels. In addition, approximately half of the coordinating molecules are fixed on the molecular wall, which also contributes to this reduced diffusion.

Our results for ion diffusion in hydrophobic and hydrophilic channels can be compared to results for particular biological channels. For example, the Na diffusion coefficient within gramicidin A[11,5] (with approximate radius 2 Å) is between 5.5×10^{-4} and 0.058 Å^2/ps. Diffusion in our 2.1 Å hydrophilic channel is approximately 29% of bulk, or, based on the experimental bulk diffusion, 0.037 Å^2/ps. Our prediction is therefore that Na ion diffusion in gramicidin A would be slightly less than this value, in agreement with the existing studies of that channel. Similarly we can compare our hydrophobic channel results to those for nAChR models. The M2 helix bundle with narrowest radius 6 Å is found to result in 2/3 of bulk Na ion diffusion.[10] Examination of Fig. 12(A) shows that our hydrophobic channel would also result in an ion diffusion coefficient of approximately 2/3 of bulk.

The study of molecular diffusion in zeolites,[3] where diffusion is a single file process, reveals two orders of magnitude reduction from bulk diffusion levels. This phenomenon is not observed in the range of pore sizes studied in this work. Even our narrowest channel (2.1 Å radius) is not small enough to result in a single-file diffusion, housing approximately 1.5 water molecules per intermolecular spacing along the channel axis direction, and as a result exhibits relatively large molecular and ion diffusion.

Our observations on the effects of pore size and constitution on ion diffusion can be related to the organization of the protein residues in the linings of transmembrane pores. The fact that axial ion diffusion is higher in hydrophobic channels than in hydrophilic ones for large pores ($R>4$ Å), and the reverse for the smaller pores ($R<4$ Å) implies existence of an optimal selection for a pore type according its size. Indeed nature tends to line wide biological transmembrane segments with nonpolar amino acids (e.g., nAChR, porins, and the wide region of the potassium channel), whereas narrow segments are lined with polar groups (such as in gramicidin A and the potassium channel selectivity filter). Our results offer realistic ion diffusion estimates for atomic and molecular pores such that ion mobility need no longer be treated as a free parameter that may be arbitrarily altered to match experimental findings.

ACKNOWLEDGMENTS

This work was supported by grants from the Australian Research Council and the National Health & Medical Research Council of Australia. The calculations upon which this work is based were partly carried out with the Silicon Graphics Power Challenge of the ANU Supercomputer Facility.

[1] B. Hille, *Ionic Channels of Excitable Membranes*, 2nd ed. (Sinauer Associates, Sunderland, MA, 1992).
[2] S. Yashonath and P. Santikary, J. Phys. Chem. **98**, 6368 (1994).
[3] K. Hahn, J. Kärger, and V. Kukla, Phys. Rev. Lett. **76**, 2762 (1996).
[4] N. Unwin, Neuron **3**, 665 (1989).
[5] B. Roux and M. Karplus, Annu. Rev. Biophys. Biomol. Struct. **23**, 731 (1994).
[6] D. A. Doyle, J. Morais Cabral, R. A. Pfuetzner, A. Kuo, J. M. Gulbis, S. L. Cohen, B. T. Chait, and R. MacKinnon, Science **280**, 69 (1998).
[7] D. P. Tieleman and H. J. C. Berendsen, Biophys. J. **74**, 2786 (1998).
[8] M. S. P. Sansom, I. D. Breed, and R. Sankaramakrishnan, Biophys. J. **70**, 693 (1996).
[9] R. M. Lynden-Bell and J. C. Rasaiah, J. Chem. Phys. **105**, 9266 (1996).
[10] G. R. Smith and M. S. P. Sansom, Biophys. J. **75**, 2767 (1998).
[11] B. Roux and M. Karplus, J. Phys. Chem. **95**, 4856 (1991).
[12] C. Y. Lee, J. A. McCammon, and P. J. Rossky, J. Chem. Phys. **80**, 4448 (1984).
[13] F. F. Abraham, J. Chem. Phys. **68**, 3713 (1978).
[14] B. R. Brooks, R. E. Bruccoleri, B. D. Olafson, D. J. States, S. Swaminathan, and M. Karplus, J. Comput. Phys. **4**, 187 (1983).
[15] L. Verlet, Phys. Rev. **159**, 98 (1967).
[16] F. H. Stillinger and A. Rahman, J. Chem. Phys. **60**, 1545 (1974).
[17] K. Heinzinger, Physica B **131**, 196 (1985).
[18] *CRC Handbook of Chemistry and Physics*, edited by D. R. Lide (CRC, Cleveland, 1994).
[19] H. J. C. Berendsen, J. R. Grigera, and T. P. Straatsma, J. Phys. Chem. **91**, 6269 (1987).
[20] W. L. Jorgensen, J. Chandrasekhar, J. D. Madura, R. W. Impey, and M. L. Klein, J. Chem. Phys. **79**, 926 (1983).
[21] V. Dagget and M. Levitt, Annu. Rev. Biophys. Biomol. Struct. **22**, 353 (1993).
[22] G. S. Del Buono, T. S. Cohen, and P. J. Rossky, J. Mol. Liq. **60**, 221 (1994).
[23] L. Perera, U. Essmann, and M. L. Berkowitz, J. Chem. Phys. **102**, 450 (1995).
[24] M. P. Allen and D. J. Tildesley, *Computer Simulation of Liquids* (Oxford University Press, New York, 1987).
[25] B. Jönsson, Chem. Phys. Lett. **82**, 520 (1981).
[26] R. Kjellander and S. Marčelja, Chem. Phys. Lett. **120**, 393 (1985).
[27] D. C. Rapaport, *The Art of Molecular Dynamics Simulation* (Cambridge University Press, Cambridge, 1995).
[28] T. W. Allen, S. Kuyucak, and S-H. Chung, Biophys. J. (in press).
[29] D. Eisenberg and W. Kauzmann, *The Structure and Properties of Water* (Oxford University Press, London, 1969).
[30] G. W. Neilson and J. E. Enderby, Annu. Rep. Prog. Chem., Sect. C: Phys. Chem. **76**, 185 (1979).
[31] S.-B. Zhu and G. W. Robinson, J. Chem. Phys. **97**, 4336 (1992).
[32] H. G. Hertz, Aqueous Solutions of Simple Electrolytes, in *Water: A Comprehensive Treatise Vol. 3*, edited by F. Franks (Plenum, New York, 1973).